Applied Surface Science 561 (2021) 149972

Contents lists available at ScienceDirect

Applied Surface Science

journal homepage: www.elsevier.com/locate/apsusc

Full Length Article

One-step plasma nitriding synthesis of Ni_xN/NF (x = 3, 4) for efficient hydrogen evolution

Guanshui Ma [a], Peng Guo [a], Shuyuan Wang [a], Yingrui Liu [a], Yang Xin [a], Hao Li [a], Rende Chen [a], Aiying Wang [a,b,*]

[a] Key Laboratory of Marine Materials and Related Technologies, Zhejiang Key Laboratory of Marine Materials and Protective Technologies, Ningbo Institute of Materials Technology and Engineering, Chinese Academy of Sciences, Ningbo 315201, China
[b] Center of Materials Science and Optoelectronics Engineering, University of Chinese Academy of Sciences, Beijing 100049, China

ARTICLE INFO

Keywords:
Ni foam
Metal nitride
Electrocatalysis
Hydrogen evolution reaction
Plasma technique

ABSTRACT

Development of high active and cost-effective non-noble metal productions was urgent for the hydrogen evolution reaction (HER) electrocatalysts in future clean energy devices. Herein, we reported a simple approach to fabrication of Ni_xN (x = 3, 4) on Ni foam (NF) through plasma-enhanced discharge nitridation in nitrogen precursors. The synthesized Ni_xN/NF cathode exhibited a remarkable electrocatalytic performance and long-term durability for the HER in alkaline condition. In view of the density functional calculations, it was further showed that introduction of N atoms in NF decreased the values of Gibbs free energy, especially the interfacial sites of Ni_4N-Ni exhibited the lowest value of −0.056 eV for H adsorption–desorption, and enhanced HER catalytic activity of Ni_xN/NF. More importantly, the synthesis approach reported here was scalable and eco-friendly, which could be used as to generate the other transition metal nitride for catalytic reaction.

1. Introduction

Nowadays, due to depleting petroleum supplies and the climate change, much attention has been paid to the development of clean and renewable energies [1]. Hydrogen (H_2), as a result of environmental friendliness and renewable properties, has been proposed to be an ideal energy carrier for hydrogen economy. To realize future hydrogen economy, efficient and convenient hydrogen generation was a basic prerequisite. Among the numerous methods for preparing hydrogen, water electrolysis represented a more renewable, cleaner and more efficient technique for hydrogen fabrication without other further problems. To enable market uptake and to deploy electrolyzers on a large scale, it was important to design and synthesis of high-performance and low-cost electrocatalysts to promote the hydrogen evolution reaction (HER) [2,3]. Up to now, many research works have been dedicated to develop HER catalysts, such as CoMo [4], W_2N [5], MoC [6,7], MoS_2 [8–19], WS_2 [20,21], MoP [22–25], Mo_2C [26–29], Co-P [30–34], and Fe-P [35,36] to replace the commonly used platinum group catalysts.

In the past several years, due to metallic nickel owned the largest HER exchange current density, lower overpotentials and faster kinetics for HER among the non-noble metals, which had attracted much attention in catalyze HER [37–39]. However, it was well known that the non-noble metal catalysts were susceptible to corrosion under strong acid or alkaline conditions and tend to aggregate into larger particles during catalytic cycling [40]. In order to set around the problem, a large number of groups had focused on Ni-N HER catalysts with different nanostructures, where the catalytic performance toward HER comprehensively was investigated [41–45]. Shalom et al.[46] prepared Ni_3N on the Ni foam (NF) matrix through solid state synthesis method, which exhibited a five-fold increase of the electrochemically active for the HER in alkaline solution than that of NF. Further, Jin and co-worker showed that upload the Ni_3N/Ni_4N heterojunction on $Zn_{0.5}Cd_{0.5}S$ could greatly delay the recombination of electron hole pairs and accelerate the migration of photocarriers for improving HER activity [47].

Although lots of methods have been now developed to prepare Ni-based HER catalysts, however, the synthetic procedures were complicated and expensive, thus leading to the final products own high cost, afterward the yield and quality of catalysts were inadequate to meet commercial requirements. In addition, their overpotential for hydrogen

* Corresponding author at: Key Laboratory of Marine Materials and Related Technologies, Zhejiang Key Laboratory of Marine Materials and Protective Technologies, Ningbo Institute of Materials Technology and Engineering, Chinese Academy of Sciences, Ningbo 315201, China.
E-mail address: aywang@nimte.ac.cn (A. Wang).

https://doi.org/10.1016/j.apsusc.2021.149972
Received 21 January 2021; Received in revised form 29 March 2021; Accepted 11 April 2021
Available online 5 May 2021

evolution and long-time stability still needs to be improved to compete with the noble metal catalysts.

Here, we reported a very facile, low cost and straightforward strategy of physical vapor process to fabricate nickel nitride (Ni_3N/Ni_4N) nanostructure on NF substrate (Ni_xN/NF, x = 3, 4), which used as cost-effective cathodes for HER with excellent performance. The cathode was specially obtained by direct plasma-enhanced nitridation of commercially available NF without any pretreatment steps and complicated chemical reactions. Moreover, compared with conventional N-atmosphere (such as azides, hydrazine, and ammonia) synthesis, the used nitrogen source of Ni_xN/NF nanostructures was N_2 precursor during physical vapor process, which was totally environmentally friendly and without any hazardous. The prepared Ni_xN/NF cathode exhibited a Tafel slope of 69 mV dec^{-1} and the best HER overpotential 97 mV at a current density of 10 mA cm^{-2}. Furthermore, the Ni_xN/NF could sustain for up to 24 h at a constant overpotential of 97 mV with only 6.5% decrease and keep its original morphology, showing good long-term durability toward HER. Density functional theory (DFT) calculations were conducted to shed light on the exceptional performance of Ni_xN/NF. It was showed that the interfacial sites of Ni_3N–N and Ni_4N–Ni have smaller values of Gibbs free energy (ΔG_{H^*}) for H adsorption–desorption, which were very close to the ideal value of 0 eV.

2. Materials and experimental methods

2.1. Preparation of Ni_xN/NF

The synthesis of Ni_xN on NF, Ni_xN/NF (x = 3, 4) electrocatalysts was carried out in a home-made physical vapor ion beam deposition equipment. NF was purchased from Changsha Lyrun New Material Co., Ltd, China (110 ppi, 0.3 mm thick). Prior to nitriding, NF with an area of 2.0 cm × 3.0 cm were washed sequentially by acetone, alcohol and deionized water. After dried with nitrogen gas, the Ni foams were loaded into the vacuum chamber of ion beam deposition equipment and subjected to the nitrogen plasmas for the in-situ synthesis of Ni_xN. Nitrogen plasma was produced by ion beam with voltage of −2500 V. The substrate negative bias voltage was −500 V, and the temperature was set at 500 °C during nitriding process. The NF was nitriding with different time (4, 8, 12, 16 h) and the obtained samples were named Ni_xN/NF-4, Ni_xN/NF-8, Ni_xN/NF-12 and Ni_xN/NF-16, respectively.

2.2. Characterization of Ni_xN/NF samples

The microstructure of the Ni_xN/NF was characterized by scanning electron microscope (SEM). The phase structure of prepared samples was performed on the X-ray diffraction (XRD) measurements with Cu Kα radiation (λ = 1.54056 Å). The high-resolution transmission electron microscopy (HRTEM) analysis was carried out on a field emission transmission electron microscopy using in a Talos F200 at the operating voltage of 200 keV. The chemical composition of the Ni_xN/NF samples was characterized by X-ray photoelectron spectroscopy (XPS).

2.3. Electrochemical characterization of Ni_xN/NF and NF

All electrochemical characterizations of samples were performed in a conventional three-electrode system by the Gamry electrochemical workstation at temperature ~25 °C. The electrolyte was 1 M KOH. The as prepared Ni_xN/NF and NF as the working electrodes, a graphite stick as the counter electrode and an Ag/AgCl electrode as the reference electrode. Linear sweep voltammetry (LSV) was performed at a scan rate of 10 mV s^{-1}. All the potentials in the experiment were calibrated to a reversible hydrogen electrode (RHE) from the following equation:

$$E(RHE) = E(Ag/AgCl) + 0.194 + 0.05916 \times pH \quad \text{(S1)}$$

The electrochemical stability of the catalyst was evaluated by chronoamperometry test under a constant overpotential of 97 mV for 24 h. Moreover, all polarization curves without iR-corrected.

2.4. DFT calculations

All the pristine and adsorption models were simulated based DFT calculations via Vienna ab-initio simulation package (VASP) code. The projector-augmented wave (PAW) approach was implemented [48,49]. The generalized gradient approximation (GGA) Perdew-Burke-Ernzerhof (PBE) exchange–correlation function was applied. The cut-off energy of the plane-wave basis was set as 400 eV. The Brillouin zone was sampled by Monkhorst-Pack k-point mesh centered at the Γ point, along with the reciprocal lattice spacing ≤ 0.03 $Å^{-1}$. The structure relaxation was carried out until it reached the convergence tolerance, *i.e.* the energy and force on each atom were respectively 1×10^{-4} eV/atom and 0.05 eV/Å. The valence electron configurations were $1s^1$ of H, $2s^2 2p^3$ of N and $3d^8 4s^2$ of Ni. The optimized Ni or Ni_4N or Ni_3N bulk cells were used to construct surface slab models. The ΔG_{H^*} was expressed as [43]

$$\Delta G_{H^*} = \Delta E_{H^*} + \Delta E_{ZPE} - T\Delta S \quad \text{(S2)}$$

where ΔE_{H^*} was adsorption energy at each hydrogen adsorption site, ΔE_{ZPE} was the difference of the zero-point energy between the adsorbed hydrogen and hydrogen in the gas phase, and ΔS was entropy change of H* adsorption. Because of the entropy of hydrogen in absorbed state could not be ignored, ΔS could be employed as $-1/2\ S_0$ (S_0 is the entropy of H_2 in the gas phase at normal situation, 1 bar of H_2 and pH = 0 at 300 K). Thus, the free energy corresponding to the adsorbed state could be written as:

$$\Delta G_{H^*} = \Delta E_{H^*} + 0.24\ eV \quad \text{(S3)}$$

The ΔE_{H^*} could be calculated by:

$$\Delta E_{H^*} = E_{sur-H} - E_{sur} - 1/2E_{H2} \quad \text{(S4)}$$

where $E_{sur\text{-}H}$ was the energy of slab with adsorbed hydrogen atom, E_{sur} was the energy of clean slab and E_{H2} was the of molecular H_2 in the gas phase.

3. Results and discussion

Fig. 1 showed the synthesis procedures of Ni_xN/NF (x = 3, 4), and the details synthesis steps were given in material synthesis section. The pretreated NF was loaded into the physical vapor ion beam deposition equipment and subjected to the nitrogen plasma for different time (The detail synthesis conditions was showed in Table S1, supplementary information (SI)). Following the plasma-enhanced discharge nitridation, the surface of the NF changed to a little black from the initial bright silver (Fig. S1, SI). The SEM images of bare NF exhibited the typical sub-micron-scaled three-dimensional (3D) skeleton structure and smooth surface (Fig. S2, SI). After nitridation treatment, the Ni_xN (x = 3, 4) array with well-preserved morphology were successfully prepared (Fig. 2). At the beginning, particles formed on the surface of NF, and as the nitriding time increased, the particles gradually became larger and more, until entire surfaces of the NF were covered. At the same time, the particles changed from round shape to peak-shapes gradually. Compared with smooth pristine NF, it was clearly that the Ni_xN/NF covered with peak-shapes array could increase the specific surface area.

In order to validate the crystallographic structures, the Ni_xN/NF-12 and NF were performed by XRD showed in Fig. 3a. All diffraction peaks of the Ni_xN/NF-12 showed that the prapared Ni_xN was composed of Ni_3N (PDF# 10-0280) and Ni_4N (PDF# 36-1300). The observed 2θ values at 38.94, 42.14, 58.51, 70.61 and 78.31 were corresponding to the (1 1 0), (0 0 2), (1 1 2), (3 0 0) and (1 1 3) of Ni_3N, and those at 41.81 and 70.91 were attributed to the (1 1 1) and (2 2 0) of Ni_4N, respectively. In addition, the XRD patterns of Ni_xN/NF-4, Ni_xN/NF-8 and Ni_xN/NF-16 were also provided (Fig. S3, SI). XPS was further supplied to research the

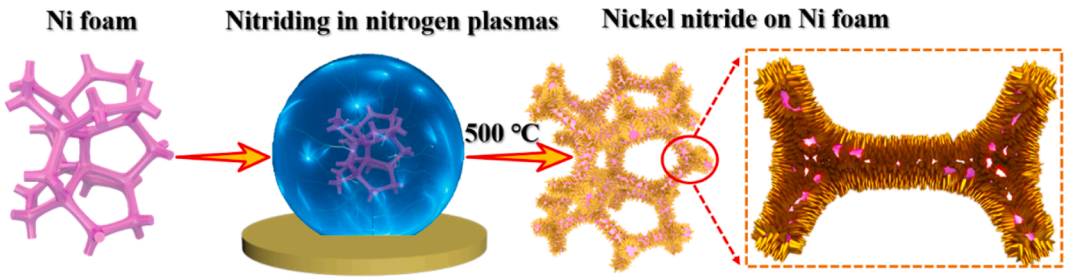

Fig. 1. A schematic of the preparation process for the Ni_xN/NF (x = 3, 4).

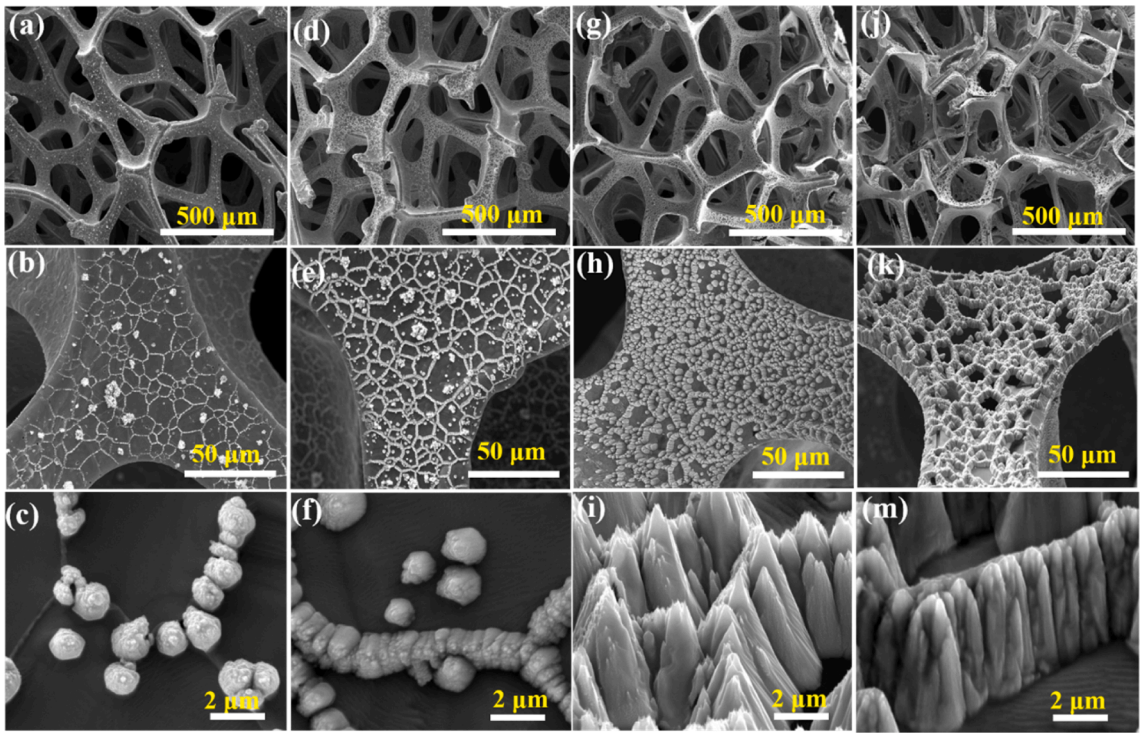

Fig. 2. SEM characterization of Ni foam after nitriding with (a-c) 4 h, (d-f) 8 h, (g-i) 12 h, (j-m) 16 h.

chemical composition and chemical valence states of the sample. From Fig. 3b, it was obviously that a typical N 1s was demonstrated at the peaks of 397.8 eV corresponded to the N–Ni bonds [50,51]. Fig. 3c showed the Ni 2p spectra, two peaks at 855.3 and 872.8 eV along with two satellite peaks at 861.1 eV and 879.5 eV were observed, which were corresponded to Ni $2p^{3/2}$ and Ni $2p^{1/2}$ of Ni^{+}, respectively [47]. Moreover, the less valence state of Ni (Ni < 1 +) was appeared at 852.5 eV ($2p^{3/2}$) and 869.5 eV ($2p^{1/2}$) [43]. The emergence of Ni < 1 + suggested that the nitriding products not just contained Ni_3N, which matched well with results in XRD.

To further investigate the detail structure of the prepared catalyst, Fig. 3d presented the HRTEM images of Ni_xN/NF-12. It was clearly seen that the lattice spacings of 0.203 nm corresponding to (0 1 1) planes of Ni were observed. The spacing of 0.214 nm and 0.231 nm assigned to the (0 0 2) and (1 1 0) plane of hexagonal Ni_3N. In addition, the lattice spacing of 0.216 nm unambiguously assigned to (1 1 1) planes of Ni_4N were also observed. Fig. 3e and f showed the results of bright-field scanning TEM and energy dispersive X-ray (EDX) analysis, presenting that the Ni and N elements were clearly observed. To further demonstrate the distribution of the elemental distribution of Ni_xN/NF-12, we used high-angle annular dark-field TEM (HAADF-TEM) and EDX mapping to characterize the sample (Fig. 3g–i). The elemental mappings clearly showed that the Ni and N elements distributed homogeneously, which revealed that the prepared Ni_xN was uniform in composition. In summary, based on the XRD, XPS, and TEM characterizations, it has been clearly demonstrated that the Ni_xN/NF (x = 3, 4) have been successfully fabricated by one step nitridation of commercially NF.

To exhibit the advantages of the as-prepared catalysts, the electrocatalytic performance for HER of the Ni_xN/NF under different nitriding time were evaluated. In Fig. 4a, the typical LSV curves for Ni_xN/NF along with bare NF for comparison. It was common knowledge that the overpotential at the current density of 10 mA cm^{-2} (η_{10}) was equivalent to 12.3% efficiency of a solar water-splitting device, so η_{10} was usually used to compare the performance of different catalysts, and a smaller η_{10} suggested a higher activity. Among the prepared samples, the Ni_xN/NF-12 demonstrated the lowest overpotential of η_{10} = 97 mV, which was much lower than Ni_xN/NF-4 (η_{10} = 124 mV), Ni_xN/NF-8 (η_{10} = 103 mV), Ni_xN/NF-16 (η_{10} = 118 mV) and as well as bare NF (η_{10} = 212 mV) (detailed data in Table S2, SI). And this was a marked low value compared with Ni-based catalysts as reported in previous literatures (Table S3, SI). As known to all, further increased potential in the cathodic potential resulted to a sharp rise in the current. The current densities of 20 mA cm^{-2} (η_{20}) were also shown, the value order of the as prepared samples and NF were in accordance with the η_{10} results (Table S2, SI). It was suggested that the Ni_xN/NF-12 had an overwhelming advantage in HER among the prepared Ni_xN/NF and NF,

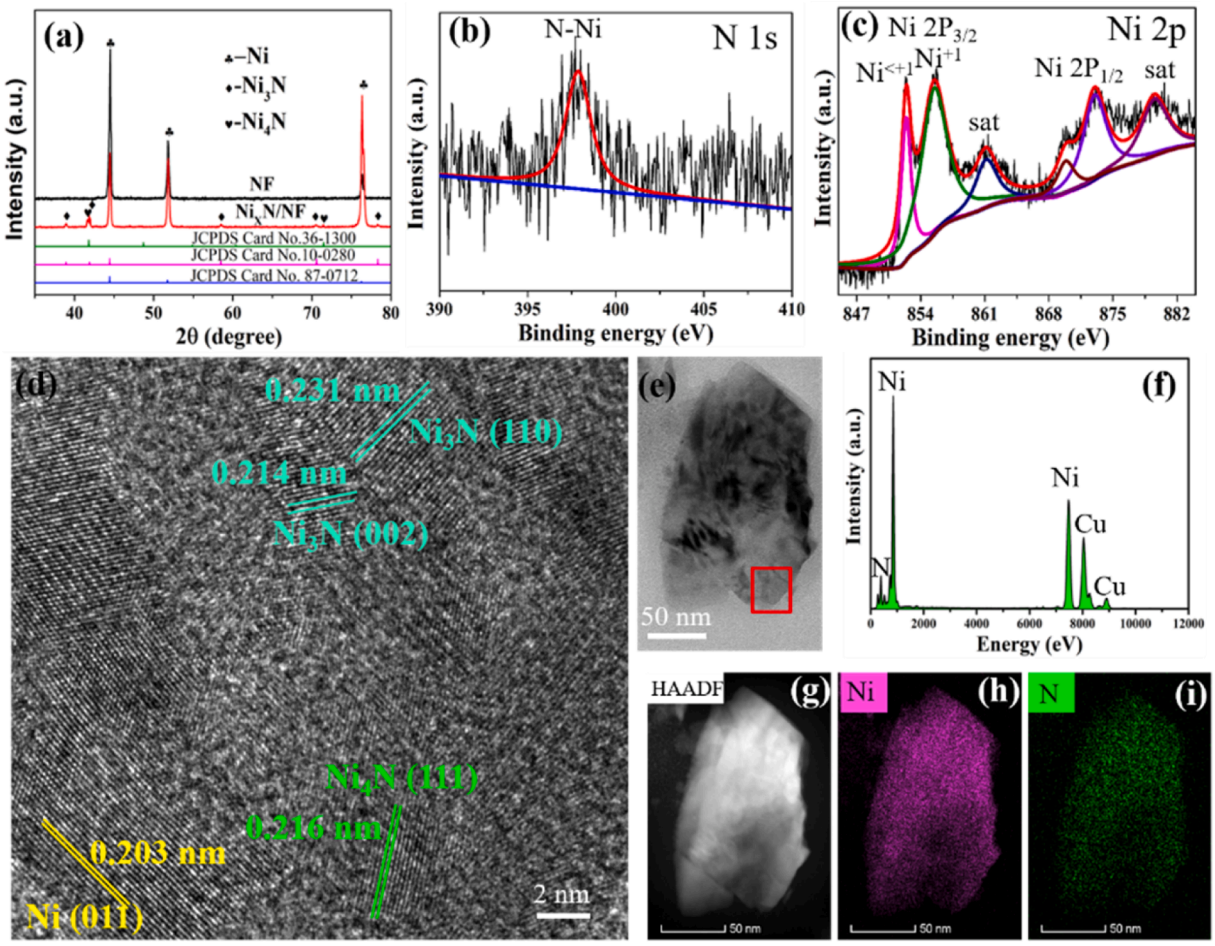

Fig. 3. Characterization of Ni_xN/NF-12 (x = 3, 4) (a) XRD, (b) and (c) XPS spectra, (d) HRTEM image, (e) TEM bright-field image, (f)~ (i) EDX pattern and HADDF-EDX element mapping of Ni_xN/NF-12.

which might be related to the surface full of peak-shapes structures with the largest specific surface area. It was obviously that NF after nitriding with 4 h, there were only a few particles on the surface (Fig. 2a-c), but the macro-porous morphology remains unchanged. When the time of nitriding change to 8 h, the more particles on the surface of NF than that of Ni_xN/NF-4 but not enough to cover the entire surface (Fig. 2d-f). Therefore, we guessed that the nucleation of grains needed a certain amount of energy and time. However, the NF after nitriding with 16 h (Fig. 2j-m), the NF collapsed and unable to maintain the original 3D skeleton structure, which led to a smaller specific surface area. To give insight the change of specific surface area, the Brunauer-Emmett-Teller (BET) surface areas of as-synthesized catalysts were detected (Table S4, SI). The result showed that the Ni_XN/NF-12 owned the largest specific surface area (6.2433 m^2/g), which was about 4.2 times that of NF (1.4669 m^2/g).

In order to evaluate the reaction kinetics of the samples, Fig. 4b presented the HER Tafel plots of the NF and the prepared Ni_xN/NF. The linear regions of Tafel curves were fitted by the Tafel equation: $\eta = a + b\ \log(j)$ (where a, b, and j were Tafel constant, Tafel slope and current density), yielded apparent Tafel slopes of 195, 164, 73, 69 and 156 $mVdec^{-1}$ for the NF, Ni_xN/NF-4, Ni_xN/NF-8, Ni_xN/NF-12 and Ni_xN/NF-16 (Table S2, SI). As expected, the Ni_xN/NF-12 exhibited the smallest Tafel slope, which was better than previous reported electrocatalysts (Table S3, SI). Furthermore, as known to all that the Tafel slope between at the scope of 40–120 mV dec^{-1}, meaning that the reaction of the Ni_xN/NF-12 follow the Volmer–Heyrovsky regulation (Fig. 6c) [2,31,52]. In addition, to further obtain insight into the HER process and mechanism with the Ni_xN/NF, electrochemical impedance spectroscopy (EIS) characterization of the Ni_xN/NF and NF cathodes were performed at an overpotential of η = 200 mV (Fig. 4c). As shown in Nyquist plots, Ni_xN/NF-12 exhibited the smallest charge transfer resistance, which suggested a highly efficient in the HER process as well as fast electronic transmission. The result was in good agreement with the observation of LSV curves and Tafel plots.

In addition to the catalytic activity, stability was another important indicator to be evaluated for the potential practical applications of a HER catalyst. Fig. 4d presented that Ni_xN/NF-12 could maintain η_{10} = 97 mV for 24 h with only 6.5% reduction, showing the excellent durability. In order to clearly understand the working situation of Ni_xN/NF-12 catalyst, digital photos of the evolution of hydrogen bubble from the catalyst surface performed at the potential of −0.58 V were shown (Fig. S4). It was obviously that there was no hydrogen bubbles evolution on the catalyst surface before voltage supply, and the electrolyte around was transparent (Fig. S4a). Contrary, when the power was switched on, the hydrogen bubbles were intensively generated from the electrode surface (Fig. S4b). For further investigate the stability of the Ni_xN/NF-12 catalyst, the surface morphology after the LSV and CA mode was characterized by SEM (Fig. S5). It obviously that the catalyst still maintains a good 3D frame structure, and more interesting is that the peak-shapes remained on the surface (The substance in the red circle may be KOH that has not been cleaned).

Gaining insight into the mechanisms of HER was not only of scientific importance but also beneficial for rationally guiding the design of high-performance catalysts. In order to shed light on the superior activity of Ni_xN/NF (X = 3, 4) as a HER electrocatalyst, DFT calculations were performed on model systems. The detailed parameters and method for

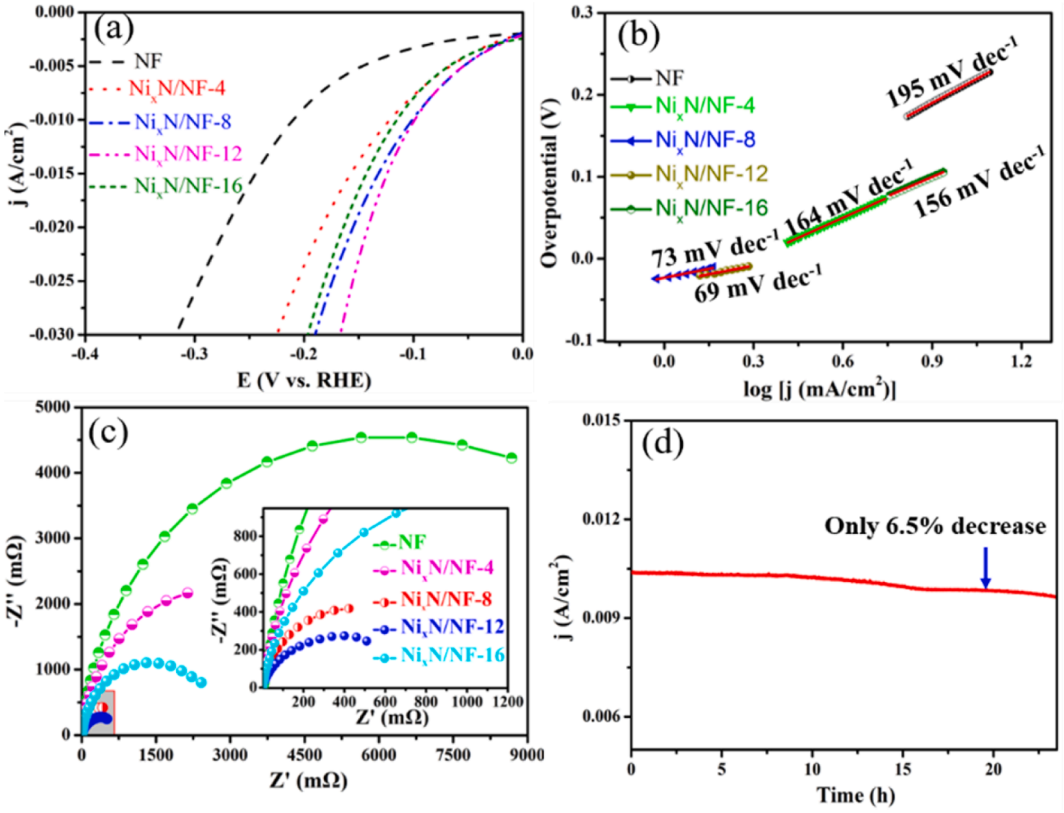

Fig. 4. HER performance of the Ni_xN/NF (x = 3, 4) (a) Linear sweep voltammetry, (b) Tafel plots, (c) Nyquist plots of Ni_xN/NF-4, Ni_xN/NF-8, Ni_xN/NF-12, Ni_xN/NF-16 and the bare Ni foam at an overpotential of 200 mV in 1 mol L^{-1} KOH with the frequency range of 10^5–0.01 HZ. (d) Chronoamperometry curve of Ni_xN/NF-12 at a constant overpotential of 97 mV.

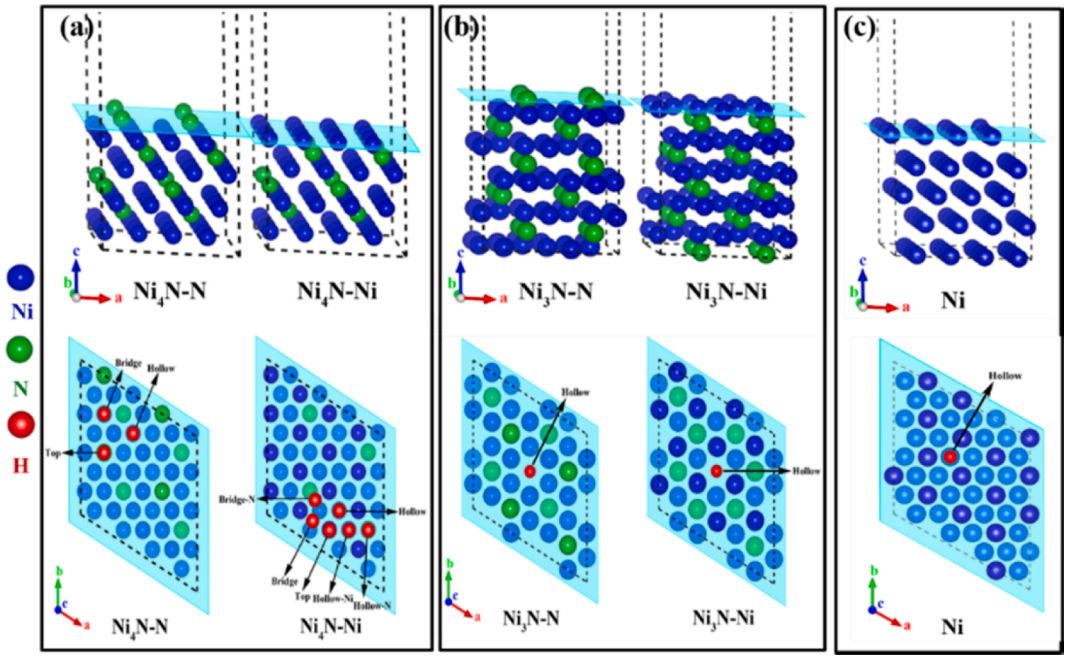

Fig. 5. (a) Adsorption sites of Ni_4N-N and Ni_4N-Ni. (b) Adsorption sites of Ni_3N-N and Ni_3N-Ni. (c). Adsorption sites of Ni.

the calculations were shown in DFT calculations. (1 1 1) lattice plane of Ni_4N was selected for simulation according to the HRTEM and XRD results. Thus, the slab sliced along (1 1 1) lattice plane and terminated with Ni atoms (Ni_4N-Ni) and N atoms (Ni_4N-N) was constructed. For Ni_4N-Ni, there were six sites for the adsorption of H atom (top, bridge, bridge-N, hollow, hollow-Ni and hollow-N), while there were three sites for Ni_4N-N (top, bridge and hollow) (Fig. 5a). According to previous report [41,53], we reasoned an appropriate structure for Ni_3N and Ni. For Ni_3N surface, a N or Ni-terminated 2 × 2 Ni_3N (0 0 1) slab of 10 layers was constructed (Fig. 5b). Moreover, a 4 × 4 Ni (1 1 1) surface slab

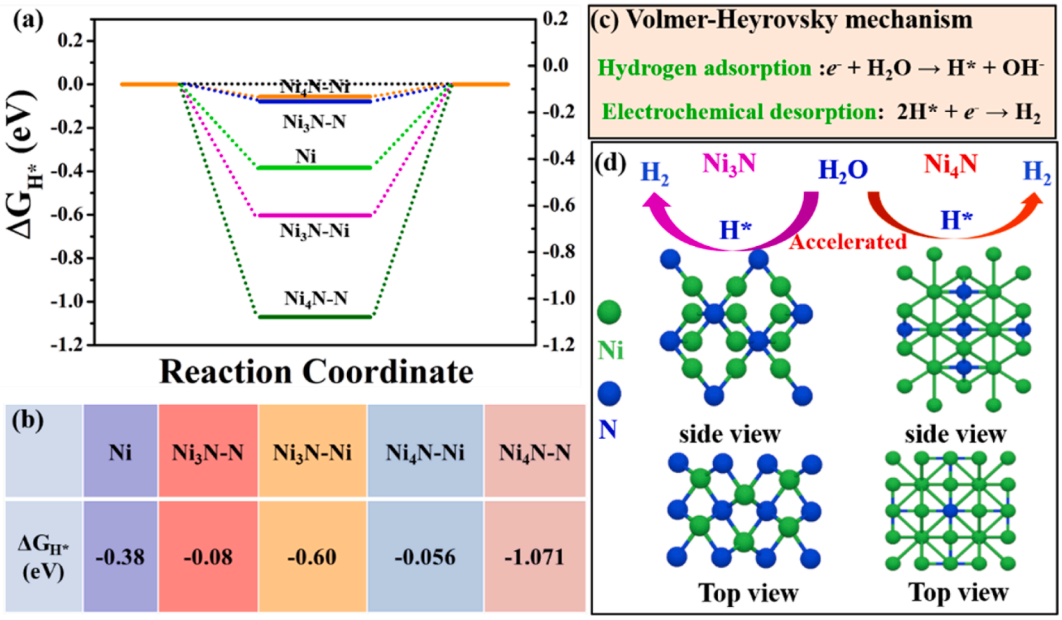

Fig. 6. Gibbs free energy (ΔG) of H* adsorption and the corresponding mechanisms of the electrocatalytic HER. H* denotes that intermediate adsorbed hydrogen. (a) and (b) The calculated free-energy diagram of HER at the equilibrium potential for catalyst samples. (c) A representative HER pathway by the Volmer-Heyrovsky mechanism. (d) Elucidation of the enhanced HER mechanism by the Ni_3N and Ni_4N.

model of 5 layers was also present, with the bottom 2 layers of atoms fixed to simulate Ni bulk (Fig. 5c). All the adsorption H* are settled at 3-fold hollow site.

In view of the Sabatier principle [54], the catalyst possessed a moderate ΔG_{H^*} could show excellent hydrogen evolution performance. The closer the ΔG_{H^*} to zero, the better advantage to both the H* adsorption and H_2 desorption process for the hydrogen evolution [55]. The resulting changes ΔG_{H^*} of Ni_4N-Ni, Ni_4N-N, Ni_3N-Ni, Ni_3N-N and Ni were calculated (Table S5, SI), as presented in Fig. 6a and b. The calculated results clearly showed that the Ni_3N and Ni_4N provided the smaller ΔG_{H^*} than that of Ni (-0.384 eV), especially the Ni_4N-Ni gave the lowest ΔG_{H^*} of −0.056 eV. In other word that because of Ni_xN composed of Ni_4N, the catalytic activities of the Ni_xN/NF further improved. The DFT simulations showed no difference with the experimental results that Ni_xN/NF (x = 3, 4) owned a significantly improved HER performance (including significantly Tafel slope and reduced overpotential) comparable to the NF in basic condition. Fig. 6d showed the diagrammatic sketch of the enhanced HER mechanism by the Ni_3N and Ni_4N.

Based on the above results, the exceptional HER electrocatalytic activity of the Ni_xN/NF might be ascribed. At first, compared with the smooth NF, the catalyst owned the 3D microporous full covered with particles or peak-shapes array, which not only increased the contact area with the solution but also maximized the number of exposed active sites. Second, the intercalation of negatively charged nitrogen atoms into metal Ni could expand the metal lattice and broaden the d-band, which gave priority to increase the contraction of the d-band and the density of states (DOS) near the Fermi level [56,57], the redistributions of the DOS were beneficial to enhance the electrocatalytic activity. Third, the prepared Ni_xN composed of Ni_4N and Ni_3N. Based on the nanostructure of Ni_4N and Ni_3N from Fig. 3d, we speculated that the charge redistribution occurred between Ni_4N and Ni_3N at the interface region. And the change of average valance charge for Ni site near the Ni_4N–Ni_3N interface was beneficial in transforming the electronic structure of Ni to resemble that of noble metals, which could be helpful for hydrogen desorption to improve the electrochemical activity [47]. In other words, there might that the synergistic effect between Ni_4N and Ni_3N contributed to the excellent electrochemical performance. The reasons came to the conclusion from the catalytic activities of the bicomponent Ni_xN/NF (x = 3, 4), which was higher than those of the Ni_3N from previous report [46,58].

4. Conclusions

In a summary, Ni_xN (x = 3, 4) on NF were successfully synthesized by a one-step route via direct nitriding method using nitrogen discharge plasma in physical vapor deposition system. This novel method for the synthesis of the Ni-based nitrides enabled an intimate contact between the active materials and the electrode substrate. The fabricated Ni_xN/NF (x = 3, 4) exhibited an excellent catalytic performance used as a cathode for HER in alkaline condition. The DFT theoretical calculations confirmed that Ni_3N and Ni_4N possessed smaller ΔG_{H^*} than that of Ni for both the H* adsorption and H_2 desorption, which were account to the enhanced HER catalytic performance of Ni_xN/NF. Moreover, the direct nitridation of NF by N_2 offered a simple and low-cost approach to synthesis HER cathodes compared with previous methods. This novel method could be readily up-scaled and eco-friendly, because of the cost-effectiveness and commercial availability both of NF and N_2. More importantly, the method could be easily extended to synthesize other metal nitride used for catalytic reaction.

Credit authorship contribution statement

Guanshui Ma: Conceptualization, Validation, Formal analysis, Investigation, Data curation, Writing - original draft, Visualization. **Peng Guo:** Investigation, Data curation, Writing - review & editing, Visualization, Project administration. **Shuyuan Wang:** Investigation, Data curation, Writing - review & editing. **Yingrui Liu:** Software, Investigation, Formal analysis. **Yang Xin:** Investigation. **Hao Li:** Software, Investigation. **Rende Chen:** Investigation, Methodology. **Aiying Wang:** Resources, Writing - review & editing, Visualization, Project administration, Funding acquisition.

Declaration of Competing Interest

The authors declare that they have no known competing financial interests or personal relationships that could have appeared to influence the work reported in this paper.

Acknowledgements

The work was supported by National Key R&D Program of China (2017YFB0702303) and K. C. Wong Education Foundation (GJTD-2019-13).

Appendix A. Supplementary material

The comparison of macroscopic morphology of porous Ni foam before and after nitriding; the SEM characterization of Ni foam; the digital photos of the situation without and with H_2 bubbles emergence on the surface of Ni_xN/NF catalyst during the chronoamperometric experiment; XRD patterns of Ni_xN/NF-4, Ni_xN/NF-8 and Ni_xN/NF-16; the surface morphological of the Ni_xN/NF-12 catalyst after chronoamperometric process. Supplementary data to this article can be found online at https://doi.org/10.1016/j.apsusc.2021.149972.

References

[1] M. Wang, W. Zhang, F. Zhang, Z. Zhang, B. Tang, J. Li, X.G. Wang, Theoretical expectation and experimental implementation of in situ Al-doped CoS_2 nanowires on dealloying-derived nanoporous intermetallic substrate as an efficient electrocatalyst for boosting hydrogen production, ACS Catal. 9 (2019) 1489–1502.
[2] X.G. Wang, Y.V. Kolen'ko, X.Q. Bao, K. Kovnir, L. Liu, One-step synthesis of self-supported nickel phosphide nanosheet array cathodes for efficient electrocatalytic hydrogen generation, Angew. Chem. Int. Ed. 54 (2015) 8188–8192.
[3] J. Zheng, W. Zhou, T. Liu, S. Liu, C. Wang, L. Guo, Homologous NiO//Ni_2P nanoarrays grown on nickel foams: a well matched electrode pair with high stability in overall water splitting, Nanoscale 9 (2017) 4409–4418.
[4] J. Chen, Y. Ge, Q. Feng, P. Zhuang, H. Chu, Y. Cao, W.R. Smith, P. Dong, M. Ye, J. Shen, Nesting Co_3Mo binary alloy nanoparticles onto molybdenum oxide nanosheet arrays for superior hydrogen evolution reaction, ACS Appl. Mater. Inter. 11 (2019) 9002–9010.
[5] V. Chakrapani, J. Thangala, M.K. Sunkara, WO_3 and W_2N nanowire arrays for photoelectrochemical hydrogen production, Inter. J. Hydrogen Energ. 34 (2009) 9050–9059.
[6] C. Wan, Y.N. Regmi, B.M. Leonard, Molybdenum carbide as electrocatalysts for the hydrogen evolution reaction, Angew. Chem. Int. Ed. 53 (2014) 6407–6410.
[7] L. Liao, S. Wang, J. Xiao, X. Bian, Y. Zhang, M.D. Scanlon, X. Hu, Y. Tang, B. Liu, H. H. Girault, A nanoporous molybdenum carbide nanowire as an electrocatalyst for hydrogen evolution reaction, Energy Environ. Sci. 7 (2014) 387–392.
[8] J. Zhang, Y. Wang, J. Cui, J. Wu, Y. Li, T. Zhu, H. Kang, J. Yang, J. Sun, Y. Qin, Y. Zhang, P.M. Ajayan, Y. Wu, Water-soluble defect-rich MoS_2 ultrathin nanosheets for enhanced hydrogen evolution, J. Phys. Chem. Lett. 10 (2019) 3282–3289.
[9] Y. Yin, J. Han, Y. Zhang, X. Zhang, P. Xu, Q. Yuan, L. Samad, X. Wang, Y. Wang, Z. Zhang, P. Zhang, X. Cao, B. Song, S. Jin, Contributions of phase, sulfur vacancies, and edges to the hydrogen evolution reaction catalytic activity of porous molybdenum disulfide nanosheets, J. Am. Chem. Soc. 138 (2016) 7965–7972.
[10] Y. Xu, L. Wang, X. Liu, S. Zhang, C. Liu, D. Yan, Y. Zeng, Y. Pei, Y. Liu, S. Luo, Monolayer $MoS_2$with S vacancies from interlayer spacing expanded counterparts for highly efficient electrochemical hydrogen production, J. Mater. Chem. A 4 (2016) 16524–16530.
[11] T. Wang, L. Liu, Z. Zhu, P. Papakonstantinou, J. Hu, H. Liu, M. Li, Enhanced electrocatalytic activity for hydrogen evolution reaction from self-assembled monodispersed molybdenum sulfide nanoparticles on an Au electrode, Energy Environ. Sci. 6 (2013) 625–633.
[12] D. Wang, Z. Pan, Z. Wu, Z. Wang, Z. Liu, Hydrothermal synthesis of MoS_2 nanoflowers as highly efficient hydrogen evolution reaction catalysts, J. Power Sources 264 (2014) 229–234.
[13] Y. Wan, Z. Zhang, X. Xu, Z. Zhang, P. Li, X. Fang, K. Zhang, K. Yuan, K. Liu, G. Ran, Y. Li, Y. Ye, L. Dai, Engineering active edge sites of fractal-shaped single-layer MoS_2 catalysts for high-efficiency hydrogen evolution, Nano Energy 51 (2018) 786–792.
[14] Y. Tan, P. Liu, L. Chen, W. Cong, Y. Ito, J. Han, X. Guo, Z. Tang, T. Fujita, A. Hirata, M.W. Chen, Monolayer MoS_2 films supported by 3d nanoporous metals for high-efficiency electrocatalytic hydrogen production, Adv. Mater. 26 (2014) 8023–8028.
[15] Y. Li, H. Wang, L. Xie, Y. Liang, G. Hong, H. Dai, MoS_2 nanoparticles grown on graphene: an advanced catalyst for the hydrogen evolution reaction, J. Am. Chem. Soc. 133 (2011) 7296–7299.
[16] Z. Bo, W. Zhu, W. Ma, Z. Wen, X. Shuai, J. Chen, J. Yan, Z. Wang, K. Cen, X. Feng, Vertically oriented graphene bridging active-layer/current-collector interface for ultrahigh rate supercapacitors, Adv. Mater. 25 (2013) 5799–5806.
[17] J. Hu, B. Huang, C. Zhang, Z. Wang, Y. An, D. Zhou, H. Lin, M.K.H. Leung, S. Yang, Engineering stepped edge surface structures of MoS_2 sheet stacks to accelerate the hydrogen evolution reaction, Energy Environ. Sci 10 (2017) 593–603.
[18] L. Yang, Q. Fu, Y.F. Huang, J.Y. Zhang, X.D. Cui, Z.Y. Fan, K.H. Liu, B. Xiang, Single-crystal atomic-layered molybdenum disulfide nanobelts with high surface activity, ACS Nano 9 (2015) 6478–6483.
[19] T.F. Jaramillo, K.P. Jørgensen, J. Bonde, J.H. Nielsen, S. Horch, I. Chorkendorff, Identification of active edge sites for electrochemical H_2 evolution from MoS_2 nanocatalysts, Science 37 (2007) 100–102.
[20] D. Voiry, H. Yamaguchi, J. Li, R. Silva, D.C. Alves, T. Fujita, M. Chen, T. Asefa, V. B. Shenoy, G. Eda, M. Chhowalla, Enhanced Catalytic activity in strained chemically exfoliated ws_2 nanosheets for hydrogen evolution, Nat. Mater. 12 (2013) 850–855.
[21] M.A. Lukowski, A.S. Daniel, C.R. English, F. Meng, A. Forticaux, R.J. Hamers, S. Jin, Highly active hydrogen evolution catalysis from metallic WS_2 nanosheets, Energy Environ. Sci. 7 (2014) 2608–2613.
[22] P. Xiao, M.A. Sk, L. Thia, X. Ge, R.J. Lim, J.Y. Wang, K.H. Lim, X. Wang, Molybdenum phosphide as an efficient electrocatalyst for the hydrogen evolution reaction, Energy Environ. Sci. 7 (2014) 2624–2629.
[23] J.M. McEnaney, J.C. Crompton, J.F. Callejas, E.J. Popczun, A.J. Biacchi, N. S. Lewis, R.E. Schaak, Amorphous molybdenum phosphide nanoparticles for electrocatalytic hydrogen evolution, Chem. Mater. 26 (2014) 4826–4831.
[24] Z. Xing, Q. Liu, A.M. Asiri, X.P. Sun, Closely interconnected network of molybdenum phosphide nanoparticles: a highly efficient electrocatalyst for generating hydrogen from water, Adv. Mater. 26 (2014) 5702–5707.
[25] W. Zhu, C. Tang, D. Liu, J. Wang, A.M. Asiri, X.P. Sun, Self-standing nanoporous MoP_2 nanosheet array: an advanced Ph-universal catalytic electrode for the hydrogen evolution reaction, J. Mater. Chem. A 4 (2016) 7169–7173.
[26] G. Zhou, Q. Yang, X. Guo, Y. Chen, Q. Yang, L. Xu, D. Sun, Y. Tang, Coupling molybdenum carbide nanoparticles with N-doped carbon nanosheets as a high-efficiency electrocatalyst for hydrogen evolution reaction, Inter. J. Hydrogen Energ. 43 (2018) 9326–9333.
[27] Y. Zhu, G. Chen, Y. Zhong, W. Zhou, M. Liu, Z. Shao, An Extremely active and durable Mo_2C/graphene-like carbon based electrocatalyst for hydrogen evolution reaction, Mater. Today Energy 6 (2017) 230–237.
[28] R. Ma, Y. Zhou, Y. Chen, P. Li, Q. Liu, J. Wang, Ultrafine molybdenum carbide nanoparticles composited with carbon as a highly active hydrogen-evolution electrocatalyst, Angew. Chem. Int. Ed. 54 (2015) 14723–14727.
[29] C. Ge, P. Jiang, W. Cui, Z. Pu, Z. Xing, A.M. Asiri, A.Y. Obaid, X.P. Sun, J. Tian, Shape-controllable synthesis of Mo_2C nanostructures as hydrogen evolution reaction electrocatalysts with high activity, Electrochim. Acta 134 (2014) 182–186.
[30] Q. Liu, J. Tian, W. Cui, P. Jiang, N. Cheng, A.M. Asiri, X.P. Sun, Carbon nanotubes decorated with Cop nanocrystals: a highly active non-noble-metal nanohybrid electrocatalyst for hydrogen evolution, Angew. Chem. Int. Ed. 53 (2014) 6710–6714.
[31] Z. Huang, Z. Chen, Z. Chen, C. Lv, M.G. Humphrey, C. Zhang, Cobalt phosphide nanorods as an efficient electrocatalyst for the hydrogen evolution reaction, Nano Energy 9 (2014) 373–382.
[32] Z. Pu, Q. Liu, P. Jiang, A.M. Asiri, A.Y. Obaid, X.P. Sun, CoP nanosheet arrays supported on a Ti plate: an efficient cathode for electrochemical hydrogen evolution, Chem. Mater. 26 (2014) 4326–4329.
[33] E.J. Popczun, C.G. Read, C.W. Roske, N.S. Lewis, R.E. Schaak, Highly active electrocatalysis of the hydrogen evolution reaction by cobalt phosphide nanoparticles, Angew. Chem. Int. Ed. 53 (2014) 5427–5430.
[34] Y. Ji, L. Yang, X. Ren, G. Cui, X. Xiong, X.P. Sun, Nanoporous CoP_3 nanowire array: acid etching preparation and application as a highly active electrocatalyst for the hydrogen evolution reaction in alkaline solution, ACS Sustain. Chem. Eng. 6 (2018) 11186–11189.
[35] P. Jiang, Q. Liu, Y. Liang, J. Tian, A.M. Asiri, X.P. Sun, A cost-effective 3d hydrogen evolution cathode with high catalytic activity: FeP nanowire array as the active phase, Angew. Chem. Int. Ed. 53 (2014) 12855–12859.
[36] Y. Xu, R. Wu, J. Zhang, Y. Shi, B. Zhang, Anion-exchange synthesis of nanoporous FeP nanosheets as electrocatalysts for hydrogen evolution reaction, Chem. Commun. 49 (2013) 6656–6658.
[37] S.H. Ahn, S.J. Hwang, S.J. Yoo, I. Choi, H.J. Kim, J.H. Jang, S.W. Nam, T.H. Lim, T. Lim, S.K. Kim, J.J. Kim, Electrodeposited Ni dendrites with high activity and durability for hydrogen evolution reaction in alkaline water electrolysis, J. Mater. Chem. 22 (2012).
[38] S.A. Abbas, M.I. Iqbal, S.H. Kim, K.D. Jung, Catalytic activity of urchin-like Ni nanoparticles prepared by solvothermal method for hydrogen evolution reaction in alkaline solution, Electrochim. Acta 227 (2017) 382–390.
[39] T. Sun, C. Zhang, J. Chen, Y. Yan, A.A. Zakhidov, R.H. Baughman, L. Xu, Three-dimensionally ordered macro-/mesoporous Ni as a highly efficient electrocatalyst for the hydrogen evolution reaction, J. Mater. Chem. A 3 (2015) 11367–11375.
[40] J. Zhu, L. Hu, P. Zhao, L.Y.S. Lee, K.Y. Wong, Recent advances in electrocatalytic hydrogen evolution using nanoparticles, Chem. Rev. 120 (2020) 851–918.
[41] F. Song, W. Li, J. Yang, G. Han, P. Liao, Y. Sun, Interfacing nickel nitride and nickel boosts both electrocatalytic hydrogen evolution and oxidation reactions, Nat. Commun. 9 (2018) e4531.
[42] Q. Zhao, Y. Li, Y. Li, K. Huang, Q. Wang, J. Zhang, Hierarchical hybrid of Ni_3N/N-doped reduced graphene oxide nanocomposite as a noble metal free catalyst for oxygen reduction reaction, Appl. Surf. Sci. 400 (2017) 245–253.
[43] B. Liu, B. He, H.Q. Peng, Y. Zhao, J. Cheng, J. Xia, J. Shen, T.W. Ng, X. Meng, C. S. Lee, W. Zhang, Unconventional nickel nitride enriched with nitrogen vacancies as a high-efficiency electrocatalyst for hydrogen evolution, Adv. Sci. 5 (2018) 1800406.
[44] S. Hu, C. Feng, S. Wang, J. Liu, H. Wu, L. Zhang, J. Zhang, Ni_3N/NF as bifunctional catalysts for both hydrogen generation and urea decomposition, ACS Appl. Mater. Inter. 11 (2019) 13168–13175.

[45] D. Gao, J. Zhang, T. Wang, W. Xiao, K. Tao, D. Xue, J. Ding, Metallic Ni_3N nanosheets with exposed active surface sites for efficient hydrogen evolution, J. Mater. Chem. A 4 (2016) 17363–17369.
[46] M. Shalom, D. Ressnig, X. Yang, G. Clavel, T.P. Fellinger, M. Antonietti, Nickel nitride as an efficient electrocatalyst for water splitting, J. Mater. Chem. A 3 (2015) 8171–8177.
[47] Z. Jin, T. Wei, F. Li, Q. Zhang, L. Xu, Fabrication of a novel Ni_3N/Ni_4N heterojunction as a non-noble metal co-catalyst to boost the H_2 evolution efficiency of Zn0.5VCd0.5S, New J. Chem. 44 (2020) 3471–3477.
[48] G. Kresse, Efficient iterative schemes for ab initio total-energy calculations using A plane-wave basis set, Phys. Rev. B 54 (1996) 169–186.
[49] G. Kresse, J. Hafner, Ab initio molecular dynamics for open-shell transition metals, Phys. Rev. B 48 (1993) 13115–13118.
[50] M. Chen, J. Qi, D. Guo, H. Lei, W. Zhang, R. Cao, Facile synthesis of sponge-like Ni_3N/NC for electrocatalytic water oxidation, Chem. Commun. 53 (2017) 9566–9569.
[51] A.N. Cloud, L.M. Davis, G.S. Girolami, J.R. Abelson, Low-temperature CVD of iron, cobalt, and nickel nitride thin films from bis [Di (Tert-Butyl) Amido] metal (II) precursors and ammonia, J. Vac. Sci. Techno. A 32 (2014) 020606.
[52] A.R.J. Kucernak, V.N. Sundaram, Nickel phosphide: the effect of phosphorus content on hydrogen evolution activity and corrosion resistance in acidic medium, J. Mater. Chem. A 2 (2014) 17435–17445.
[53] Z.W. Seh, J. Kibsgaard, C.F. Dickens, I. Chorkendorff, J.K. Norskov, T.F. Jaramillo, Combining theory and experiment in electrocatalysis: insights into materials design, Science 355 (2017) 1.
[54] Y.Y. Ma, C.X. Wu, X.J. Feng, H.Q. Tan, L.K. Yan, Y. Liu, Z.H. Kang, E.B. Wang, Y. G. Li, Highly efficient hydrogen evolution from seawater by a low-cost and stable CoMoP@C electrocatalyst superior to Pt/C, Energy Environ. Sci. 10 (2017) 788–798.
[55] J. Yu, A. Li, L. Li, X. Li, X. Wang, L. Guo, Morphological and structural engineering in amorphous Cu_2MoS_4 nanocages for remarkable electrocatalytic hydrogen evolution, Sci. China Mater. 62 (2019) 1275–1284.
[56] J.G. Chen, Carbide and nitride overlayers on early transition metal surfaces: preparation, characterization, and reactivities, Chem. Rev. 96 (1996) 1477–1498.
[57] S. Dong, X. Chen, X. Zhang, G. Cui, Nanostructured transition metal nitrides for energy storage and fuel cells, Coordin. Chem. Rev. 257 (2013) 1946–1956.
[58] Y. Wang, L. Chen, X. Yu, Y. Wang, G. Zheng, Superb alkaline hydrogen evolution and simultaneous electricity generation by Pt-decorated Ni_3N nanosheets, Adv. Energy Mater. 7 (2017) 1601390.